PNAS
www.pnas.org

Supplementary Information for

Room-temperature autonomous self-healing glassy polymers with hyperbranched structure

Hao Wang, Hanchao Liu, Zhenxing Cao, Weihang Li, Xin Huang, Yong Zhu, Fangwei Ling, Hu Xu, Qi Wu, Yan Peng, Bin Yang, Rui Zhang, Olaf Kessler, Guangsu Huang, and Jinrong Wu[1]

[1] Corresponding author
Email: wujinrong@scu.edu.cn

This PDF file includes:

Materials and Methods
Theoretical calculation
Figures S1 to S10
Tables S1 to S5
SI References

Other supplementary materials for this manuscript include the following:

Movies S1

Supplementary Information Text

Materials and Methods

Materials. *N,N'*-methylene diacrylamide (MBA, 99+%) and Methanol (99.9%) were purchased from Adamas. 1,4-Butanediamine (BDA, 98+%) was purchased from Alfa Aesar. Acetone and deionized water were purchased from Chengdu Kelong Chemical Reagent Factory. All the chemicals were used as received without further purification.

Synthesis of regular hyperbranched polymers. The randomly hyperbranched polymers (RHP) were synthesized by one-pot method through Michael addition reaction between MBA and BDA at different molar ratios. The materials were denoted as RHP-x, where x 1, 2, 3 correspond to MBA/BDA molar ratios of 1/1.125, 1/1 and 1/0.875, respectively. In a typical procedure, the synthesis of RHP-1 was described as follows: MBA (12.332 g, 0.08 mol) was added into a round bottom flask equipped with a magnetic stirrer containing mixed solvent of 60 mL methanol and 30 mL deionized water at 30 ℃ and stirred until it was dissolved totally. Then BDA (8 g, 0.09 mol) was dissolved in a beaker containing mixed solvent of 20 mL methanol and 10 mL deionized water and fed into the flask directly. The mixture was stirred at 30 ℃ for 24 h. After that, the solution was poured into a beaker containing 1000 mL acetone to precipitate at room temperature. The crude product was washed 5 times with acetone to obtain a solid and then dried in a vacuum oven at 50 ℃ for 48 h.

Preparation of RHP films. In a typical process, 5 g RHP was powdered in a universal crusher, and then the powder was hot pressed under 10 MPa at 100 ℃ for 30 min in the mold. The resulting yellowish transparent film of RHP-1 was shown in Fig. 1D. We used gel permeation chromatography (GPC) to measure the molecular weight of RHP-2 after processing. The result shows that Mn=7286 g/mol and Mw=20182 g/mol for the hot pressed RHP-2, which are very close to the values of RHP-2 before processing. It indicates that the molecular weight of RHP does not change during processing.

Characterization. FTIR spectra were recorded on Nicolet iS10 (Nicolet, America) in the range of 4000-400 cm^{-1} at room temperature. The FTIR sample of RHP was formed after evaporation of methanol on a piece of KBr plate. The RHP was heated from 20 ℃ to 150 ℃ at 1 ℃/min, and the temperature-dependent FTIR spectra were collected at the same time. Moreover, we collected 21 spectra (from 20 ℃ to 40 ℃ at the heating rate of 1 ℃/min) and used 2DCS software (get the open version from http://muchong.com/t-11812062-1) to process these data, generating the generalized 2D correlation spectra. To obtain a credible result, the baseline correction was performed in the wavenumber region of 1585-1495 cm^{-1} before analysis. The ^{1}H NMR spectra were measured on a Bruker AV III HD spectrometer operating at 400 MHz in deuterated methanol solution with TMS as reference. Quantitative ^{13}C NMR spectra were measured by the method of inverse gated ^{1}H decoupling on a Bruker AV III HD spectrometer operating at 400 MHz in deuterated dimethyl sulfoxide solvent. ^{13}C, ^{1}H-HSQC spectra were recorded using the standard pulse sequence provided by Bruker. The ^{1}H NMR curves with different temperatures were measured on Bruker AVANCE IIITM HD 400 MHz spectrometer with deuterated dimethyl sulfoxide as solvent. X-ray diffraction experiments on RHP were carried out on a Rigaku X-ray diffractometer (Ultima IV) equipped with parallel beam optics attachment. X-ray diffraction of RHP at different temperatures was measured with Rigaku X-ray diffractometer (Smartlab). DSC tests were performed on a Perkin Elmer Diamond 3000 with the mass of all samples ranging from 3 mg to 8 mg. Samples were heated from -50 ℃ to 150 ℃ at a heating rate of 10 ℃/min and then cooling to -50 ℃ at 10 ℃/min. The heating and cooling processes were performed two times. DLS measurements were carried out by a wide angle laser scattering instrument (BI-200SM, Brookhaven) equipped with a cuvette rotation/translation unit (CRTU) and a He-Ne laser (22 mW, wavelength λ of 632.8 nm) to study the mean diameter of RHP. The molecular weight and polydispersity index (PDI) of the RHP were

determined by GPC at room temperature on an Agilent PLgel 5um MIXED-C gel columns with a Waters-2414 refractive index detector (DMF as the eluent). DMA tests were measured on Q800 (TA Instrument) in a tension mode with the sample dimension about 20×5×1 mm^3. Tests were performed in temperature scanning mode in the range of -20 ℃ to 150 ℃ at a ramping rate of 3 ℃ /min and a frequency of 1 Hz with a strain amplitude of 30 μm. Dielectric measurements were carried out through two different patterns on a Novocontrol Concept 50 system with Alpha impedance analyzer and Quatro Cryosystem temperature control. Frequency sweep mode used the frequency range of 10^{-1} to 10^7 Hz at each temperature from -60 to 100 ℃ with 10 ℃ interval, with temperature stability better than 0.1 K. The disk-shaped film with 1 mm thickness and 20 mm in diameter was placed into two parallel electrodes. Mechanical properties were performed on an Instron 5967 tensile tester at room temperature with a strain rate of 10 mm/min. The dumbbell shaped sheets had a thin strip with central dimensions of 35×2×1 mm^3. To measure the self-healing efficiency, the dumbbell shaped specimen was cut by a razor blade, and the fresh cut surfaces were recombined by hand and then put into vacuum oven at 25 ℃ for different time. The healed sample was subjected to on stretching experiment again.

Theoretical calculation

Degree of branching (DB). The degree of branching can be calculated by the following equation (1):

$$DB = \frac{D + T}{D + T + L}$$

where D, T, L represent the fractions of the dendritic unit, terminal unit and linear unit, respectively, which are calculated by the quantitative ^{13}C NMR spectra.

Analyses of the dielectric spectra. Below T_g, the analyses of the dielectric spectra are made by using Havriliak and Negami (HN) function. In this model, the frequency dependence of the dielectric complex permittivity (ε^*) can be described by the following equation (2,3):

$$\varepsilon^*(\omega) = \varepsilon_\infty + \frac{\Delta\varepsilon}{[1 + (i\omega\tau_{HN})^\alpha]^\beta}$$

where $\Delta\varepsilon=\varepsilon_s - \varepsilon_\infty$ is the dielectric strength, ε_s and ε_∞ are the relaxed and unrelaxed values of dielectric constant, and τ_{HN} is the characteristic relaxation time. The parameters α and β ($0 < \alpha, \alpha\beta \leq 1$) define the symmetrical and asymmetrical broadening of the loss peak.

The relation between τ_{HN} and average relaxation time τ_{max} is given by the following equation:

$$\tau_{max} = \tau_{HN}\left[sin\frac{\pi\alpha\beta}{2(1+\beta)}\right]^{\frac{1}{\alpha}}\left[sin\frac{\pi\alpha}{2(1+\beta)}\right]^{-\frac{1}{\alpha}};\ f_{max} = \frac{1}{2\pi\tau_{max}}$$

where f_{max} is the frequency at which ε'' passes through the maximum value.

The relation between the average relaxation time τ_{max} and the temperature is Arrhenius-like and can be described by

$$\tau_{max} = \tau_0 exp\left(\frac{E_a}{RT}\right)$$

where E_a is the activation energy and τ_0 is a proportionality constant.

Above T_g, both real and imaginary parts of dielectric permittivity are large, the relaxation process can be distinguished from the complex dielectric modulus format. Dielectric modulus (M^*) is defined as the reciprocal of complex permittivity and can be described by (4)

$$M^*(\omega) = M'(\omega) + iM''(\omega) = \frac{1}{\varepsilon^*(\omega)} = \frac{\varepsilon'(\omega) + i\varepsilon''(\omega)}{[\varepsilon'(\omega)]^2 + [\varepsilon''(\omega)]^2}$$

We refer to the value obtained from the maximum in the dielectric loss modulus as the average relaxation time τ_{max}. This characteristic relaxation time can be correlated with the temperature through Vogel-Fulcher-Tamman (VFT) equation (5,6):

$$\tau_{max} = \tau_0 exp\left(\frac{B}{T - T_0}\right)$$

where τ_0 and B are empirical parameters and T_0 is the so-called Vogel temperature.

Self-healing efficiency. Healing efficiency (η) is calculated according to the following equation:

$$\eta = \frac{\sigma_{heal}}{\sigma_{pri}} \times 100\%$$

where σ_{heal} is the tensile strength of the healing samples, and σ_{pri} is the tensile strength for the pristine samples.

Noda's rule for the generalized 2D correlation spectra

If the correlation intensity Φ(*v1*, *v2*) in synchronous spectra has the same symbol (positive or negative) as the correlation peak Ψ(*v1*, *v2*) in asynchronous spectra, then the movement of band *v1* is prior to or earlier than that of band *v2*, and vice versa. Besides, if the correlation intensity in synchronous spectra is not zero (or blank), but zero in asynchronous one, then the movements of bands at *v1* and *v2* are simultaneous.

Noda's rules are summarized as follows:

(1) If Φ(*v1*,*v2*) > 0, Ψ(*v1*,*v2*) > 0 or Φ(*v1*,*v2*) < 0, Ψ(*v1*,*v2*) < 0, then the movement of *v1* is before than that of *v2*.

(2) If Φ(*v1*,*v2*) > 0, Ψ(*v1*,*v2*) < 0 or Φ(*v1*,*v2*) < 0, Ψ(*v1*,*v2*) > 0, then the movement of *v1* is after than that of *v2*.

(3) If Φ(*v1*,*v2*) > 0, Ψ(*v1*,*v2*) = 0 or Φ(*v1*,*v2*) < 0, Ψ(*v1*,*v2*) = 0, then the movements of *v1* and *v2* are simultaneous.

Φ(*v1*,*v2*) and Ψ(*v1*,*v2*) represent the correlation peaks in synchronous and asynchronous spectra, respectively.

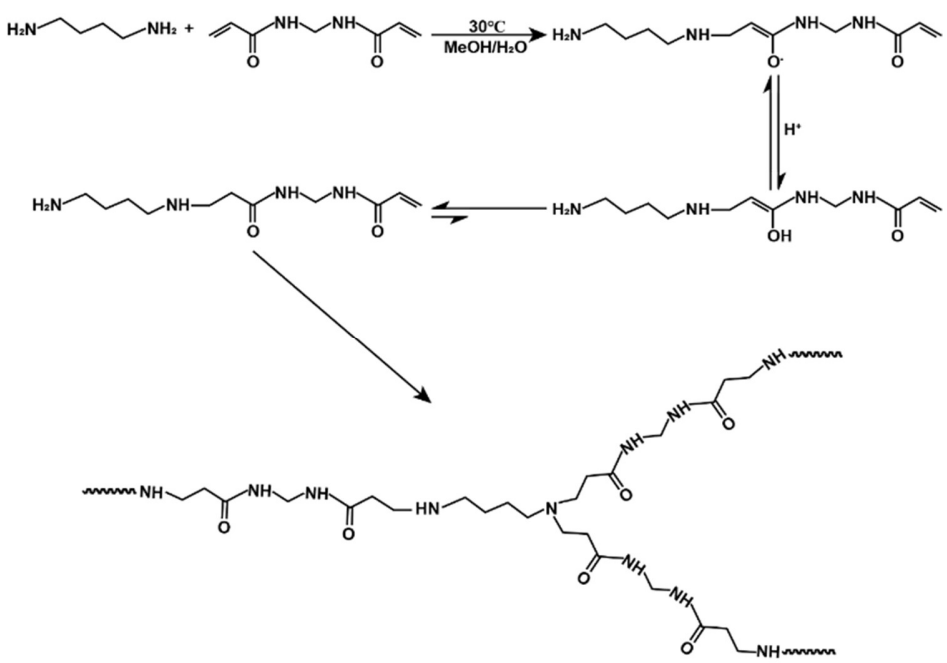

Fig. S1. Schematic diagram of synthetic reaction mechanism of RHP. The -NH- of BDA can react with a CH_2=CH- on MBA under a mild condition to fabricate RHP molecules. And the reaction can form new secondary amines and tertiary amines.

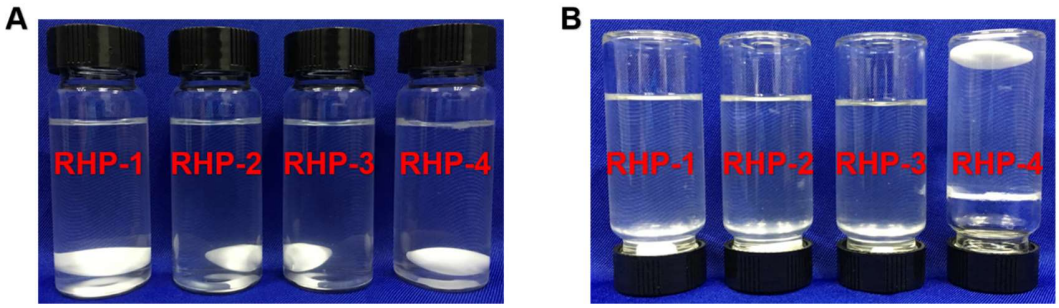

Fig. S2. Photographs showing the dissolution state of RHP in methanol/water solvent after reacting for 0 minutes (A) and 24 h (B). After reaction for 24 h, RHP-1, RHP-2 and RHP-3 with MBA to BDA ratio from 1/1.125 to 1/0.875 are soluble in the solvent, as when the vials are upside down, the solutions flow down. However, when the MBA to BDA reaches 1:0.75 in RHP-4, gelation takes place. Therefore, even when the bottle is upside down, the system cannot flow and the stirrer bar is still on the top.

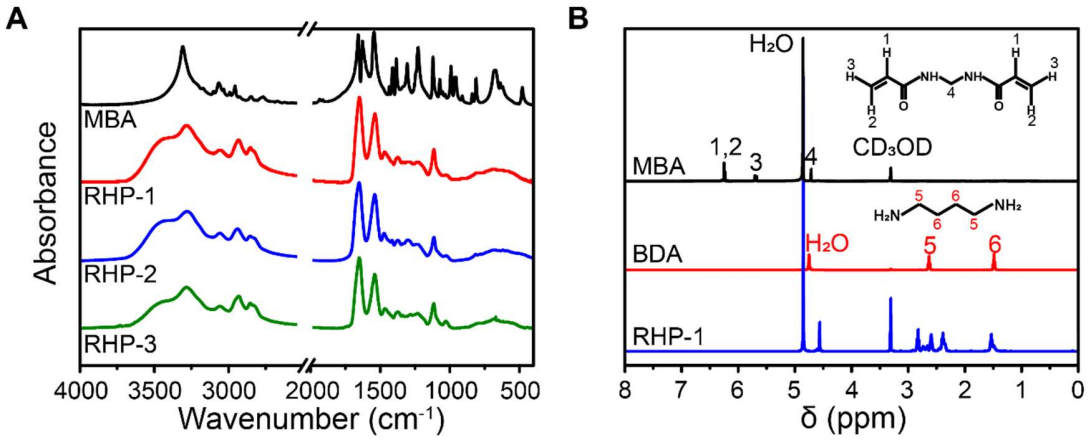

Fig. S3. FTIR and NMR analysis. (A) FTIR spectra of MBA, RBP-1, RBP-2 and RBP-3, respectively. In the FTIR spectrum of MBA, the characteristic peaks at 3305 cm^{-1}, 1658 cm^{-1}, 1543 cm^{-1} are belonged to the strong stretching vibration of N-H group, C=O stretching vibration peak and N-H bending vibration peak, respectively, while the peaks at 992 cm^{-1} and 967 cm^{-1} are assigned to the bending vibration peaks of vinyl groups (7). In RHP, the characteristic amide I band at around 1648 cm^{-1}, amide II band at around 1536 cm^{-1} and disappeared vinyl group bending vibration peak indicate that the Michael addition reaction consumes all double bonds and hyperbranched networks are successfully formed. (B) ^{1}H NMR spectra of MBA, BDA and RHP-1. The typical proton signals at 6.25 ppm and 5.70 ppm corresponding to vinyl groups disappear after reaction, while new signals appear at 2-3 ppm belonging to the methylene of $-CH_2-CH_2-CONH-$ in RHP-1. It indicates that all the vinyl groups have been consumed (8).

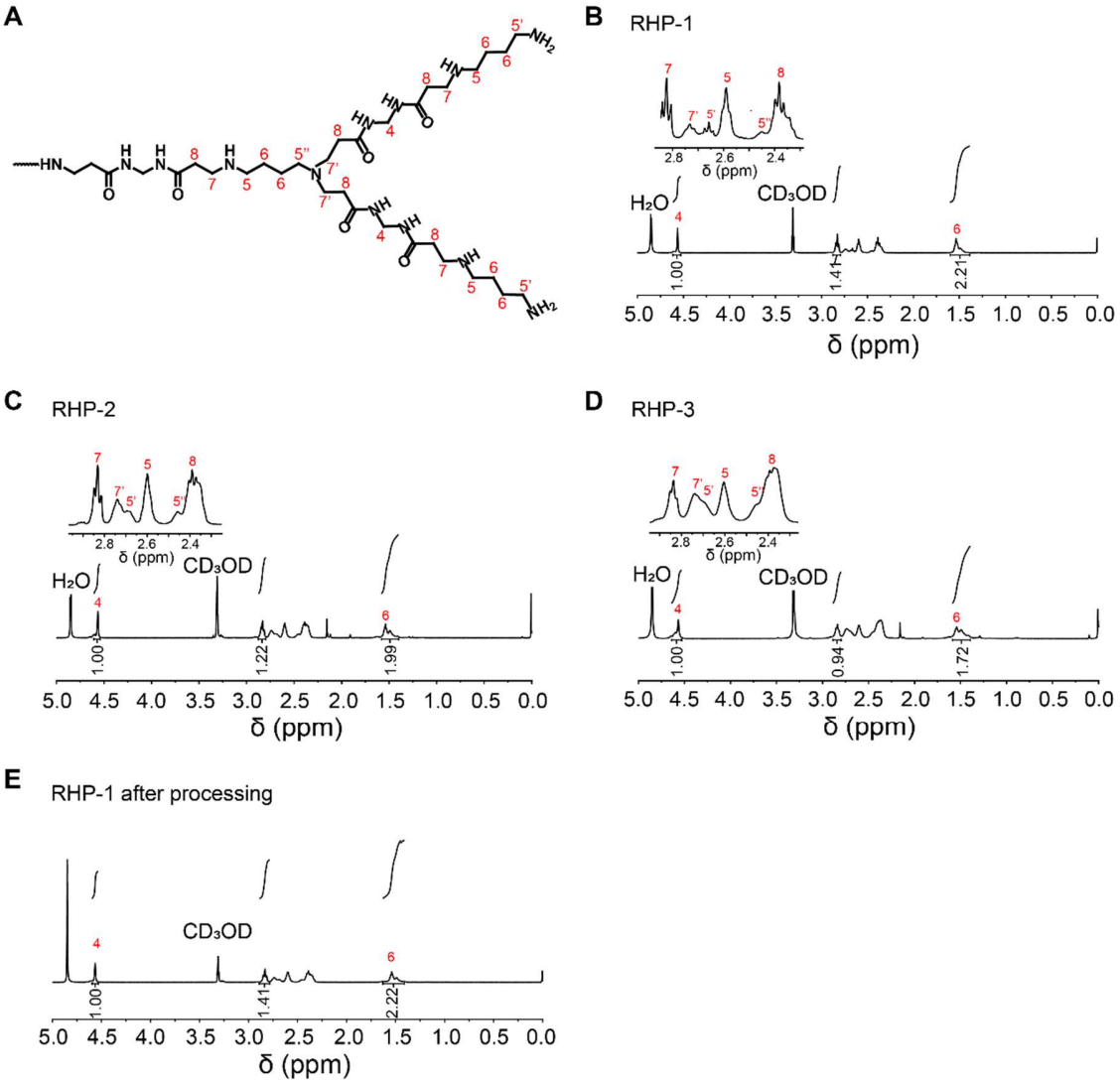

Fig. S4. Structure characterization of RHP. (A) Chemical structure of RHP. ^{1}H NMR spectrum of RHP-1 (B), RHP-2 (C) and RHP-3 (D) (400 MHz, in CD_3OD). With the molar ratio between MBA and BDA increases, the percentage of primary amine units decreases and the tertiary amine units increases (details are shown in Table S2). (E) ^{1}H NMR spectrum of RHP-1 after processing (400 MHz, in CD_3OD). The ^{1}H NMR spectrum of RHP-1 after processing is essentially the same as that before processing (Fig S4 *B*), indicating that the hyperbranched structure do not change after processing.

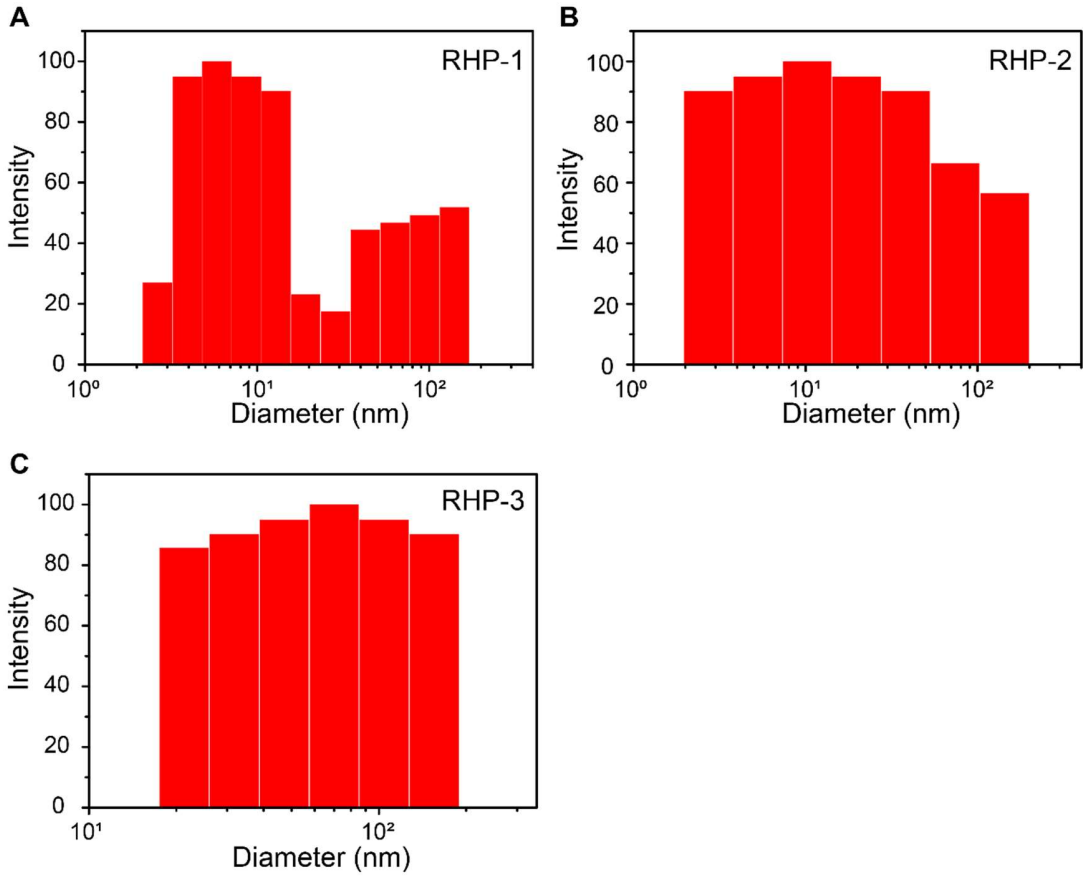

Fig. S5. DLS measurements of RHP. Size distribution of RHP-1 (A), RHP-2 (B) and RHP-3 (C) measured by DLS (details are shown in Table S3).

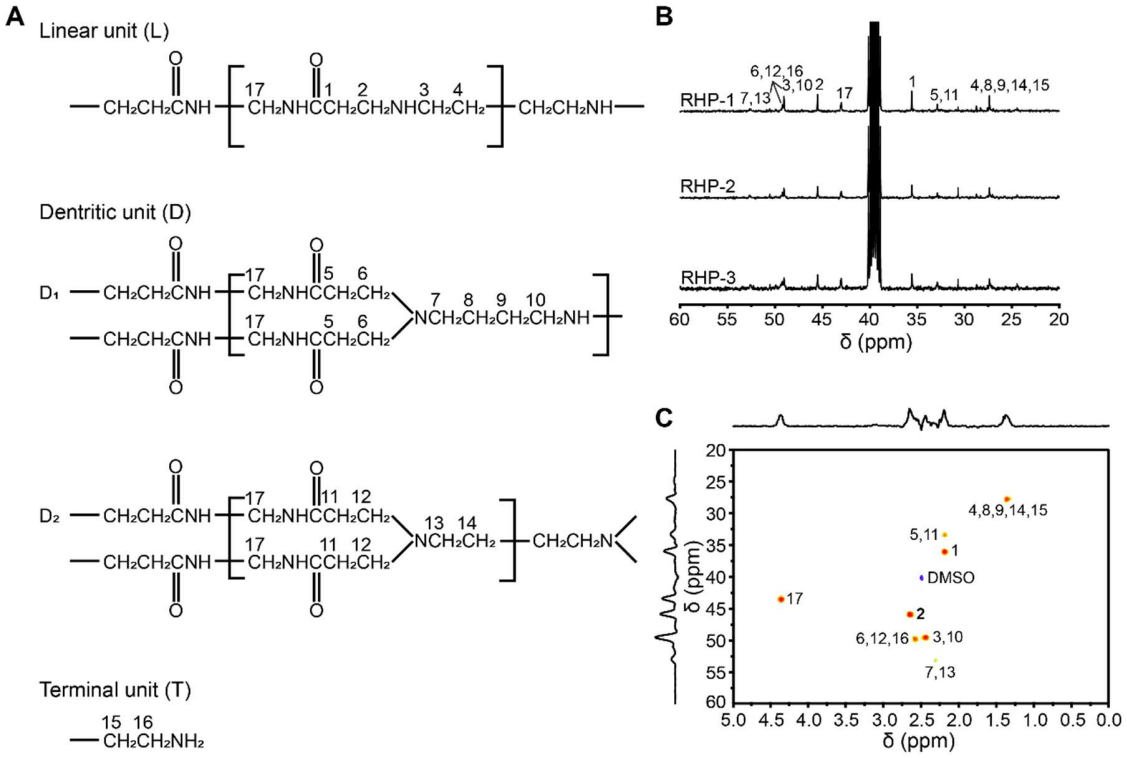

Fig. S6. Characterization of the degree of branching of RHP. (A) Structure units of the RHP. (B) Quantitative ^{13}C NMR spectra of RHP and (C) ^{13}C, ^{1}H-HSQC spectra of RHP-1. The ^{13}C, ^{1}H-HSQC spectra reveal the assignment of the structure units, and the quantitative ^{13}C NMR spectra are used to calculate the degree of branching of RHP (details are shown in Table S4).

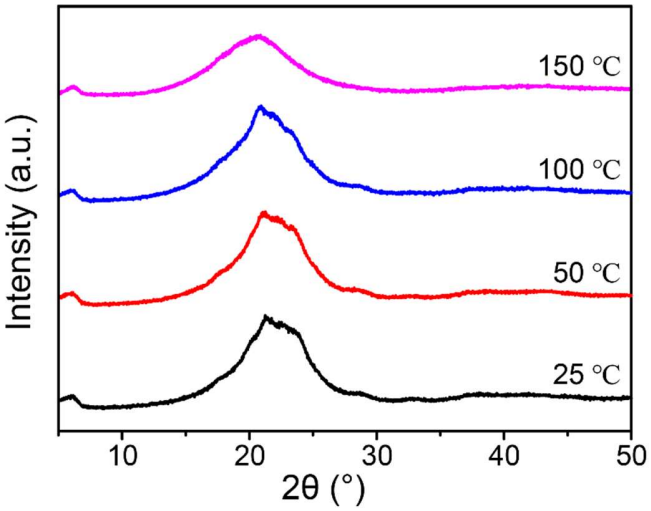

Fig. S7. Temperature-dependent XRD profile of RHP-1. The XRD profile of RHP-1 shows several weak sharp peaks in addition to the broad diffusion-like peak at room temperature, indicating the existence of crystals. These sharp peaks are stable up to 100 ℃, while disappear at 150 ℃ which is above the melting point of RHP-1, suggesting the melting of the crystals between 100 ℃ and 150 ℃.

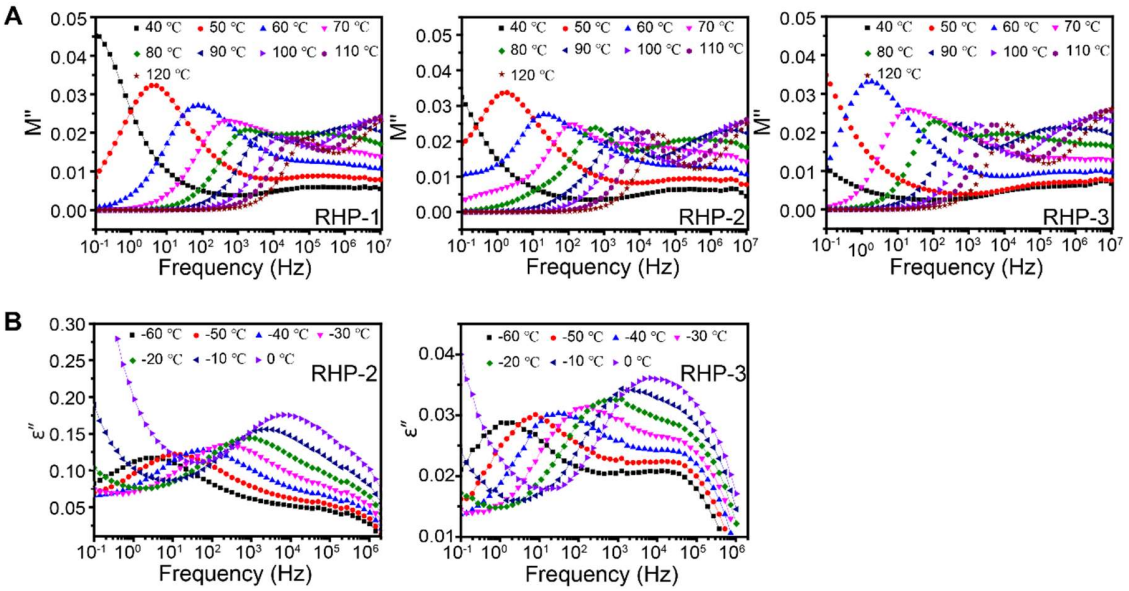

Fig. S8. Dielectric measurements of RHP above and below T_g. (A) Dielectric modulus *M"* as a function of frequency for RHP-1, RHP-2 and RHP-3 from 40 °C to 120 °C, respectively. The average relaxation time τ_{max} of α process at 25 °C was calculated by VFT equation. The τ_{max} values were in the range of 10^5 s (RHP-1) to 10^9 s (RHP-3) (details were show in Table S5). (B) Dielectric loss *ε"* as a function of frequency for RHP-2 and RHP-3 from -60 °C to 0 °C, respectively.

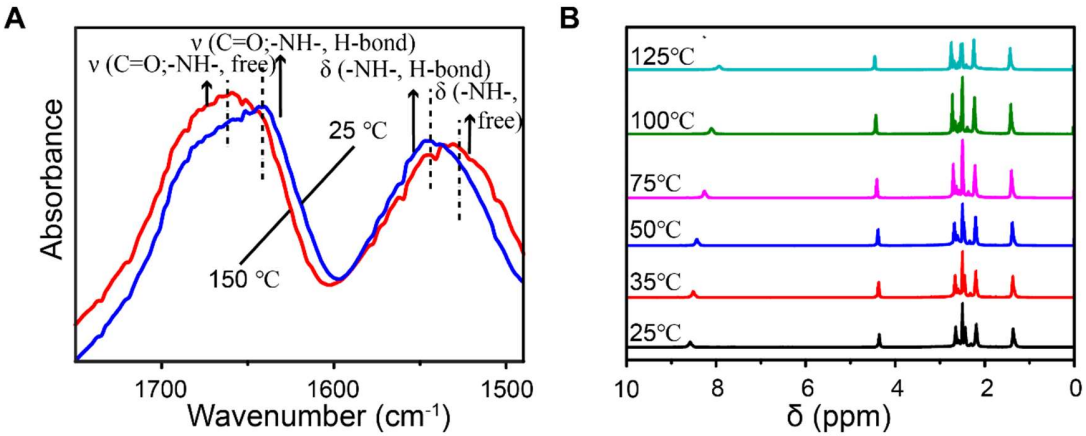

Fig. S9. Temperature-dependent FTIR and ^{1}H NMR measurement of RHP. (A) Temperature-dependent FTIR spectra of the RHP-1 upon heating at 25 °C (blue) and 150 °C (red). (B) ^{1}H NMR spectral change of RHP-1 in deuterated dimethyl sulfoxide with an increase in temperature from 25 °C to 125 °C.

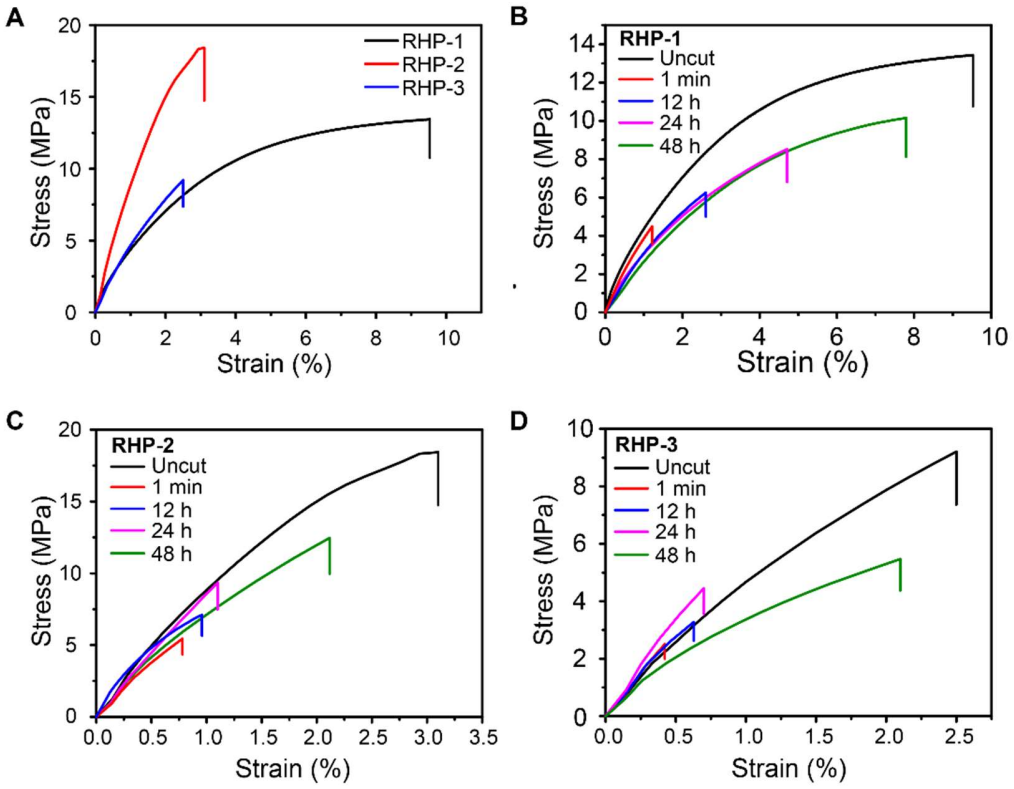

Fig. S10. Mechanical properties and self-healing tests of RHP. (A) The stress-strain curve of RHP. The representative stress-strain curves of the RHP-1 (B), RHP-2 (C) and RHP-3 (D) self-healed at 25 °C for different time.

Table S1. The feed ratio and yield of RHP.

RHP	MBA/BDA [a]	Yield (wt%) [b]
RHP-1	1:1.125	75.3%
RHP-2	1:1	84.7%
RHP-3	1:0.875	92.1%

[a] The molar ratio of MBA and BDA.
[b] Weight of the RHP obtained/weight of the monomer used.

Table S2. The mole percentage of primary amine, secondary amine and tertiary amine units.

RHP	MBA/BDA	primary amine (%)	secondary amine (%)	tertiary amine (%)
RHP-1	1:1.125	22.8	63.8	13.4
RHP-2	1:1	19.1	61.3	19.6
RHP-3	1:0.875	14.6	54.6	30.8

Table S3. The mean diameter, T_g and molecular weight of RHP.

RHP	Mean Diameter (nm)[a]	T_g (℃)[b]	Mn[c] (g/mol)	Mw[c] (g/mol)	PDI[c]
RHP-1	35.6	37	8199	14547	1.77
RHP-2	42.5	42	8091	16173	2.00
RHP-3	71.6	49	9943	23319	2.35

[a] Determined by DLS (dissolved in methanol, 0.5 g/L).

[b] Determined by DSC at a heating rate of 10 ℃/min.

[c] Determined by GPC (dissolved in DMF at room temperature).

Table S4. The DB values of RHP.

RHP	DB
RHP-1	0.16
RHP-2	0.24
RHP-3	0.33

Table S5. The VFT Parameters for Segmental Process.

RHP	τ_0	B (K)	T_0 (K)	τ_{max} (s)[a]
RHP-1	4.76×10^{-9}	1011	265.8	1.7×10^{5}
RHP-2	4.76×10^{-9}	1098	266.2	3.8×10^{6}
RHP-3	4.76×10^{-9}	1213	268.9	4.9×10^{9}

[a]The average relaxation time of segmental motion at 25 ℃.

Movie S1 (separate file). The instantaneous self-healing behavior of RHP.

SI References

1. Jia Z, Chen H, Zhu X, & Yan D (2006) Backbone-thermoresponsive hyperbranched polyethers. *J Am Chem Soc* 128:8144-8145.
2. Diaz-Calleja R (2000) Comment on the maximum in the loss permittivity for the Havriliak−Negami equation. *Macromolecules* 33:8924-8924.
3. Boersma A, Van Turnhout J, & Wübbenhorst M (1998) Dielectric characterization of a thermotropic liquid crystalline copolyesteramide: 1. Relaxation peak assignment. *Macromolecules* 31:7453-7460.
4. Sun M, Pejanović S, & Mijović J (2005) Dynamics of deoxyribonucleic acid solutions as studied by dielectric relaxation spectroscopy and dynamic mechanical spectroscopy. *Macromolecules* 38:9854-9864.
5. Ortiz-Serna P*, et al.* (2010) Dynamics of Natural Rubber as a Function of Frequency, Temperature, and Pressure. A Dielectric Spectroscopy Investigation. *Macromolecules* 43:5094-5102.
6. Tang Z*, et al.* (2014) Rational design of graphene surface chemistry for high-performance rubber/graphene composites. *Macromolecules* 47:8663-8673.
7. Pérez E, Martínez A, Teijón C, Teijón JM, & Blanco MD (2014) Bioresponsive nanohydrogels based on HEAA and NIPA for poorly soluble drugs delivery. *Int J Pharmaceut* 470:107-119.
8. Zhang J, Liang X, Zhang Y, & Shang Q (2016) Fabrication and evaluation of a novel polymeric hydrogel of carboxymethyl chitosan-g-polyacrylic acid (CMC-g-PAA) for oral insulin delivery. *RSC Adv* 6:52858-52867.